ARCHIVES
of
FOUNDRY ENGINEERING

ISSN (2299-2944)
Volume 2025
Issue 3/2025

105 – 115

12/3

10.24425/afe.2025.155359

Published quarterly as the organ of the Foundry Commission of the Polish Academy of Sciences

Effect of Fewer Strands Casting on Molten Steel Flow, Temperature Distribution, and Transition Billet Length in a 12-strand Tundish

Yali Zhang [a], Jintao Song [b], Chao Chen [b, *]
[a] Lvliang University, China
[b] Taiyuan University of Technology, China
* Corresponding author: E-mail address: chenchao@tyut.edu.cn

Received 06.02.2025; accepted in revised form 12.03.2025; available online 23.07.2025

Abstract

The present study investigates the fewer strands casting operation in an industrial 12-strand tundish. Numerical simulations are employed to analyze the effects of different fewer strands casting cases on the molten steel flow, temperature distribution, and the length of the transition billet. Cases 1 to 4 are corresponding to the situations of all strand open, closure of strand 1, closure of strand 2, and closure of both strands 1 and 2, respectively. The results show that the volume fraction of slow-flow region is ranked as follows: Case 1 < Case 3 < Case 2 < Case 4. Fewer strands casting operation slightly increases the slow-flow volume, which hinders molten steel flow at the far-side strands 5 and 6. The residence time distribution (RTD) curve and flow characteristic results indicate that the Case 2 performs better than Case 3 in fewer strands casting, while Case 4 significantly worsens the molten steel flow at the far-side strands. The maximum temperature differences for Cases 1 to 4 are 30.9 K, 26.1 K, 28.7 K, and 26.4 K, respectively. In Case 2, the temperature profile of the near-side strands exhibits better consistency than in Case 3. The average length of transition billets is ranked in the following sequence: Case 4 < Case 2 < Case 3 < Case 1. Both case 2 and case 3 result in a reduced billet length compared to the normal casting condition in case 1. In all, the Case 2 i.e. close strand 1 is the optimum case when closing one strand in fewer strands casting operation. The closing of two strands is not recommended.

Keywords: Fewer strand casting, 12-strand tundish, Transition length, Grade change, Temperature distribution

1. Introduction

Continuous casting tundish is connected between the ladle and the mold, and is the final metallurgical reactor before the solidification of molten steel [1-3]. Proper tundish operation can improve inclusion removal, temperature uniformity, and intermixing [4-9]. The multi-strand tundish is more complex due to the control of flow and temperature consistency between each strand [10-11]. The 12-strand tundish [12-13] is currently the tundish with the highest number of strands known. Due to the structural limitations of ultra-multi-strand (12-strand) tundishes, two ladle shrouds and two separate tundishes are used to match one ladle in continuous casting [12]. In practice, due to considerations regarding annual production capacity or production pace, 12-strand tundishes are often subjected to fewer

strands casting, typically involving the closure of 1-2 strands. For fewer strands casting operations, researchers have conducted extensive studies [14-20] on the flow field, temperature field, and inclusion removal rate in 4-strand and 6-strand tundishes. Numerous conclusions have been drawn by researchers regarding tundish flow characteristics, optimal strand closure schemes, and flow control device optimization. For the 12-strand tundish with the highest number of strands, fewer strands casting is more common and widely applied. Only Zhang et al. [13] studied the flow characteristics after strand closure in a 12-strand tundish, and they found that the dead zone volume increased after strand closure. In addition, they concluded that closing the near strand (strand 1) is the reasonable single-strand closure solution. Research on fewer strands operation in a 12-strand tundish is relatively rare and required.

In fast-paced production processes, when the steel compositions of the two consecutive ladles are similar, grade transition casting is employed [21-34]. Researchers have studied factors such as pouring level, casting speed, and flow control device optimization during the grade transition casting process. Physical and numerical simulation results indicate that lowering the initial pouring level in the tundish and increasing the casting speed are effective methods to reduce the length of the transition billet during grade transition operation, with the impact of initial pouring level being greater than that of casting speed [22-23]. In terms of tundish structure and flow control devices, an optimal combination of dams and weirs [24-25] along with the use of stepped tundishes [26], can also effectively reduce the length of the transition billet. During the grade transition casting process, not only the molten steel composition differs, but there are also temperature differences. The temperature difference induces thermal buoyancy and affects the flow field, which in turn affects the transition billet length. Temperature differences are also an important factor influencing the grade transition process [27-28]. Besides, during the grade transition casting process, it is crucial to ensure that the transition billet composition shifts from narrow specification steel to wide specification steel [29]. Recently, Song et al. [30-32] established a multi-field coupled three dimensional mathematical model for the grade transition process through numerical simulations, and predicted the composition of the grade transition billet. Ren et al. [33] analyzed inclusions in the grade transition billet and found an increase in number of inclusions and a significant decrease in billet cleanliness. However, during industrial production, grade transition casting is frequently operated under fewer strands casting conditions. Currently, there is no reported research on the grade transition casting process under fewer strands casting operations. It is unclear whether the length of the transition billet varies under these conditions. To avoid misjudging the transition billet length and reduce production costs, it is essential to study the grade transition casting process in the multi-strand tundish under fewer strands casting conditions.

In order to investigate the effect of fewer strands casting on molten steel flow, temperature distribution, and the grade transition casting process, this study focuses on an industrial 12-strand tundish and employs numerical simulation methods to analyze the overall flow field and slow-moving molten steel zones in the tundish, and the residence time distribution (RTD) curve, temperature variations, and transition billet length of each strand. The study will provides a theoretical basis for the fewer strands casting process in 12-strand tundishes, and offers practical references for industrial production operations.

2. Model and Methods

To study the effects of the fewer strands casting operation on molten steel flow, the temperature variation when high-temperature molten steel from the new heat is continuously injected into the lower-temperature molten steel from the previous heat, and the grade transition casting process, the flow field and temperature field were calculated independently.

2.1. Computational Fluid Dynamics Model

2.1.1. Geometric model

The 12-strand tundish is consist of two separate 6-strand tundishes. The schematic diagram of the 12-strand tundish pouring system is presented in Figure 1. This is a long tundish with inlet (ladle shroud) located at one side but not the center. The tundish dimensions measure approximately 7 meters in length and 1 meter in width. The strands from the tundish pouring area are numbered 1 to 6. The production parameters are as follows: the ladle capacity is 150 t, and the tundish capacity is 50 t. the billet cross-section is 150×150 mm and the casting speed is 2.8 m/min. For the tundish, the ladle shroud has an immersion depth of 300 mm and a diameter of 71.76 mm, while the outlet nozzle diameter is 25 mm. The tundish liquid level is maintained at 820 mm.

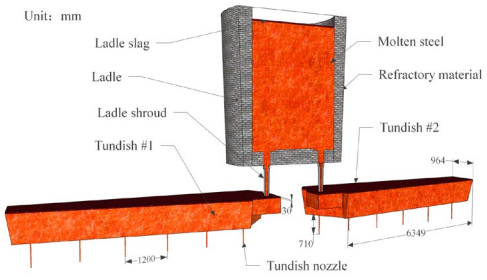

Fig. 1. Schematic diagram of the 12-strand tundish pouring system

The 1/2 model of the tundish, which is similar to a 6 strand tundish, is studied. The geometry and mesh of tundish is shown in Figure 2. The mesh of the tundish is in total of 662,278 cells. The solution of numerical model is performed in Simcenter STAR-CCM+ V2021.3 software. The realizable k-ε two layer model is used to describe the turbulent phenomena. Besides, chemical reactions are not considered. The steel melt is assumed to be incompressible fluid.

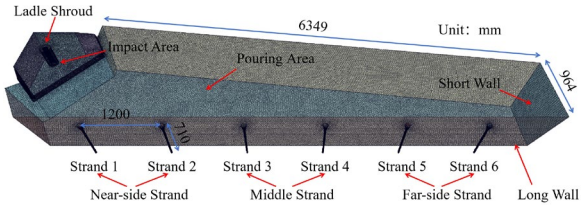

Fig. 2. Geometry and mesh of the 12-strand tundish

2.1.2. Governing equations

The flow phenomena in the tundish are described by the unified equations (1).

$$\rho\frac{\partial\phi}{\partial t}+\rho\mathbf{u}\frac{\partial\phi}{\partial x}=\frac{\partial}{\partial x}\left[\Gamma_{\phi,eff}\frac{\partial\phi}{\partial x}\right]+S_{\phi} \tag{1}$$

where ρ is the density, kg/m^3; ϕ is the solved variable, which in this study includes velocity, concentration, turbulent kinetic energy, and turbulent dissipation rate; **u** is the velocity vector, m/s; t is the time, seconds (s); $\Gamma_{\phi,eff}$ is the effective diffusion coefficient of the solved variable, m^2/s; S_{ϕ} is the source term. x is the spacial coordinate.

2.1.3. Species Transport Model

The species transport model is used to predict the transport process of a tracer as well the strand concentration during grade change in the model, and the equation in the model can be described as

$$\frac{\partial}{\partial t}(\rho\omega)+\nabla\cdot(\rho\mathbf{u}\omega)=\nabla\cdot(\rho D_{eff}\nabla\omega) \tag{2}$$

where ω is the volume fraction of the tracer in the computational domain. D_{eff} is the effective diffusion coefficient of passive scalar, m^2/s.

For the tracer transport process, the simulation process uses the 'stimulus-response' method, and the residence time distribution (RTD) curve is used to analyze the flow characteristics of the steel flow in the tundish. This is used for study the transport process of tracer as a classical chemical reactor engineering method. The overall descriptions are similar to previous work [19-20]. The pulse injection time interval of the tracer is 1 s. During the pulse injection, $\omega = 0$ in the whole region cells except the tracer injection cells, while in the tracer injection cells $\omega = 1$. After injection, the ω in the injection cells are set to 0. ω (outlet cross-section area averaged) of the outlet is used as the outlet value for the analysis of the RTD curve.

For the grade transition casting process, continuous tracer injection is used to simulate the composition change of the new heat of ladle. In the simulation, the initial concentration ω in the tundish is set to 0, and, after t=0, the concentration ω in the inlet region cells are set to 1. Afterwhile, the concentration gradually changes from 0 to 1 in the whole tundish. The changes of concentration at each strand are monitored, thus obtaining the concentration-time variation curve. In this case, the strand concentration ω represents the ratio of the concentration difference of chemical elements between the two heats during the grade transition casting process, as shown in equation (3).

$$\omega=\frac{w_S-w_P}{w_N-w_P} \tag{3}$$

where w_S, w_N, and w_P represent the mass fractions of the chemical element at the strand outlet, new heat, and present heat, respectively.

2.1.4. Heat Transfer Model

The variation of density with temperature is considered through the Boussinesq model, as shown in equation (4).

$$\rho=\rho_{st}(1-\beta\Delta T) \tag{4}$$

where, ρ_{st} is the density of molten steel, kg/m^3; β is the thermal expansion coefficient, $\beta = 9.72 \times 10^{-5}$ K^{-1}; ΔT is the temporary temperature difference, ℃.

To simplify the analysis, this study does not investigate the temperature drop process of the two heats of molten steel. The temperatures of the two heats are set to 1793 K and 1844 K, respectively. The specific simulation process for the ladle changeover process is as follows: the initial temperature is set to 1793 K, and the heat flux on all wall surfaces is set. After iterative calculations, the computation is stopped when all residuals are less than 1×10^{-4}, and the steady-state wall temperature distribution is obtained. The steady-state results are used as the initial conditions for the transient simulation. The actual scenario simulated is the process where, after ladle changeover process, the higher-temperature molten steel (1844 K) from the new heat is continuously injected into the lower-temperature molten steel (1793 K) in the previous heat's tundish.

2.2. Initial Conditions and Solution Details

The boundary conditions are set as follows: the solid surfaces are treated as no-slip, rough wall conditions, with a wall roughness of 0.00027; the inlet is set as a velocity inlet.

The specific parameter settings and boundary conditions are shown in Table 1. The inlet turbulent kinetic energy (k) and turbulence dissipation rate (ε) are provided in Equations (5) and (6):

$$k=\frac{3}{2}(I\mathbf{v})^2 \tag{5}$$

$$\varepsilon=\frac{C_{\mu}^{3/4}k^{3/2}}{L} \tag{6}$$

where, I is the turbulence intensity (I=0.02), **v** is the inlet velocity, C_{μ} is the proportional coefficient (C_{μ}=0.09), L is the characteristic length (L=0.07D), and D is the ladle shroud diameter.

Table 1.
Numerical simulation parameters and wall boundary conditions

Parameter	Value
Density of molten steel(kg·m^{-3})	7020
Dynamic viscosity(Pa·s)	0.005967
Inlet velocity(m·s^{-1})	1.558
Turbulent kinetic energy(J·kg^{-1})	0.001456
Turbulent dissipation rate(m^2·s^{-3})	0.001807
Free surface heat flux(kW·m^{-2})	15
Bottom wall heat flux(kW·m^{-2})	1.4
Long wall heat flux(kW·m^{-2})	3.2
Short wall heat flux(kW·m^{-2})	3.8
Internal wall (dam, weir, stopper) heat flux (kW·m^{-2})	1.75
Initial temperature (K)	1793
New heat temperature (K)	1844

The governing equations are solved based on the finite volume method using Simcenter Star-CCM+ V2021.3 software. The steady-state flow field is calculated iteratively using the RKE-2L model, and the steady-state simulation results are used as the initial conditions for the transient simulation. The pressure-velocity coupling is solved using the semi-implicit (SIMPLE) method for pressure-coupled equation sets to solve the concentration or temperature equation. The convergence criterion requires that the residuals of all variables be less than 1×10^{-4}. For the transient simulation, the time step increases gradually, with an initial time step of 0.002 s, a growth factor less than 1.25, and a maximum time step of 1 s. Each time step includes 30 iterations.

2.3 Studied Cases

The research cases presented in Table 2 was designed based on operational data from a 12-strand tundish continuous casting process at an industrial steel plant, and after reviewing relevant literature reference [13]. Case 1 is the normal or reference case, with all strands open. The strand 1 and strand 2 are closed in Case 2 and Case 3, respectively. In addition, both the strand 1 and strand 2 are closed in the Case 4.

Table 2.
Studied cases

Cases	Strand close scenarios
Case 1	all strands open
Case 2	strand 1
Case 3	strand 2
Case 4	strand 1and 2

3. Result Analysis

3.1 Mesh Independence Verification

The velocity distribution at the tundish strands for three different mesh configurations is illustrated in Figure 3. The mesh configurations, denoted as Mesh 1, Mesh 2, and Mesh 3, consist of 521,216, 662,278, and 920,611 grids, respectively. The velocity distribution along the line crossing strands 1 to 6 reveals six distinct peak values. Notably, the peak velocity initially increases and subsequently decreases. Overall, the velocity distributions for all three meshes demonstrate similar trends. Balancing simulation accuracy and computational efficiency, this study selects the mesh with 662,278 grids for further analysis. The distance between individual mesh nodes in this configuration is 0.035 m.

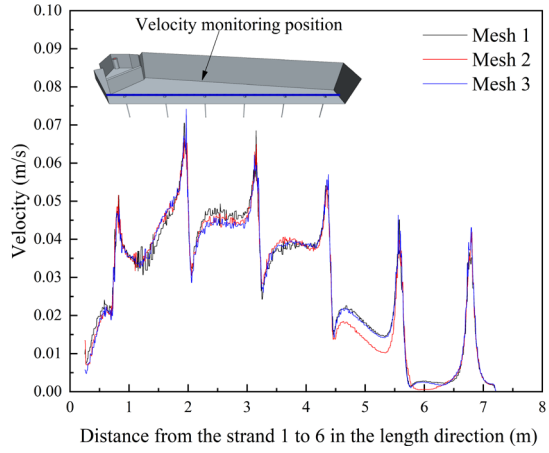

Fig. 3. Velocity distribution at the strands of tundish with different mesh numbers

3.2. Tundish flow field

The flow field results of the tundish are shown in Figure 4. As shown in Figure 4(a), the flow field in the tundish can be divided into three regions. The first is the high-speed impact region. In this region, the molten steel flows from the open area of the impact zone through the space between the strand 1 and strand 2 into the pouring area. It forms the main flow direction along the length of the tundish. The second region is in the central part of the tundish, a large circulation zone is formed and is located from the strand 2 to strand 3. Besides, a vortex is formed near strand 1 of the tundish. The third region is located around strand 4 to strand 6 in the tundish, and the steel flow forms a slow-flow region. After the molten steel passes the short wall on the right side of strand 6, a backflow forms. The slow-flow region, with the steel flow velocity less than 0.0025 m/s is visualized in Figure 4(b). This is based on the definition by He et al. [35]. Figure 5 shows the volume fraction data of the slow-flow region for each case. In Case 1, the slow-flow volume is 0.88 m^3. In Cases 2 and

3, the slow-flow volume increases to 1.13 m^3 and 1.11 m^3, respectively. In Case 4, the slow-flow volume is the largest with a value of 1.40 m^3. The volume fraction of the slow-flow region is ranked as Case 1 < Case 3 < Case 2 < Case 4. This suggests that performing fewer strands casting in the tundish increases the slow-flow volume at the far-side strand region, which hinders molten steel flow and mixing. From the volume fraction data, closing strand 2 is slightly better than closing strand 1. After closing both strands, the slow-flow volume increases significantly.

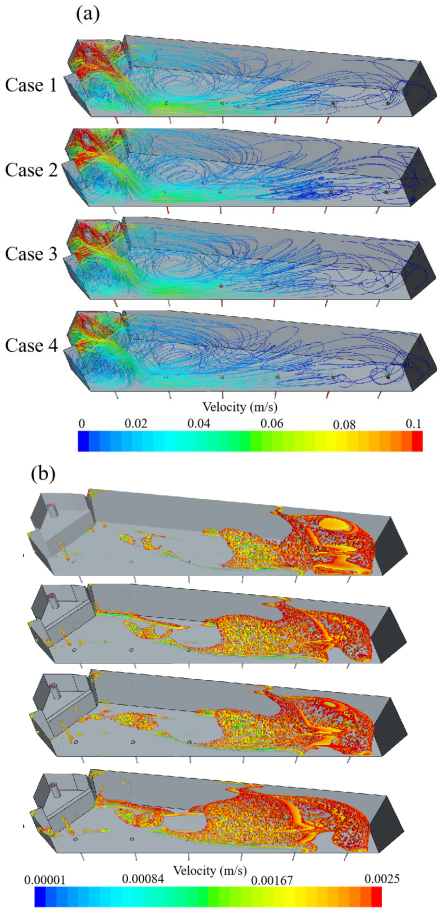

(a) Streamline figures; (b) Slow-flow region

Fig. 4. Flow field calculation results for each case in the tundish

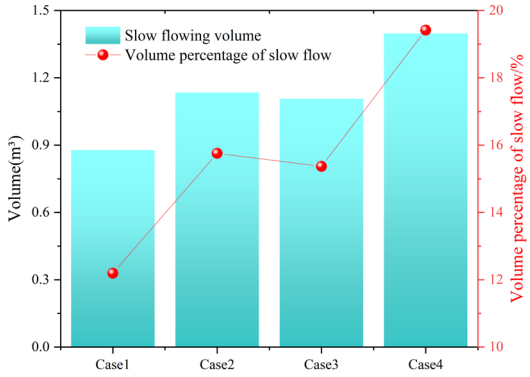

Fig. 5. Volume fraction of the slow-flow region for each case

The RTD curves at each strand further illustrates the flow characteristic and consistency of the strands. Figures 6-9 show the RTD curves at different strands for Cases 1-4, respectively. Table 3 presents the flow characteristic parameters for each case. As shown in Figures 6(a), (b), and Table 3, in the all strand open Case 1, the response time at strands 1-4 gradually increase. The minimum response times at strands 1 and 2 are 16.7s and 23.3s, with high peak concentrations of 7.85 and 9.93, respectively. The peak concentrations at strands 5 and 6 are below 1.5. The minimum response times are extremely long, the values at strands 5 and 6 are 130s and 339.5s, respectively. This phenomenon corresponds to the flow in Figure 4(b), the strands 5 and 6 are located at the slow-flow region.

Table 3.
Flow characteristic parameters of each case

Case	Parameters	Strand					
		1	2	3	4	5	6
Case 1	Minimum response time/s	16.7	23.3	43.0	68.3	130	339.5
	Peak concentration time/s	34.7	39.0	65.1	98.8	226.7	888.8
	Peak concentration	7.84892	9.93189	7.79684	4.97351	1.20712	0.61629
	Mean residence time/s	200.4	256.0	353.1	507.3	999.3	1063.9
Case 2	Minimum response time/s		27.0	50.8	80.7	138.6	377.5
	Peak concentration time/s		44.6	78	118	223.2	1177.5
	Peak concentration		10.28272	7.01653	4.89262	1.67688	0.60596

	Mean residence time/s		300.8	442.4	576.5	971.5	1314.3
Case 3	Minimum response time/s	19.6		49.9	80.1	154.8	387.6
	Peak concentration time/s	42.4		76.2	117.6	272.9	958.5
	Peak concentration	7.50878		8.37232	5.07191	1.28124	0.67533
	Mean residence time/s	276.8		436.1	605.5	1094.1	1341.5
Case 4	Minimum response time/s			64.4	105.2	191.4	503
	Peak concentration time/s			100.9	157.9	320	1245.9
	Peak concentration			7.42341	4.61376	1.43682	0.76246
	Mean residence time/s			422.8	578.8	993.9	1615.1

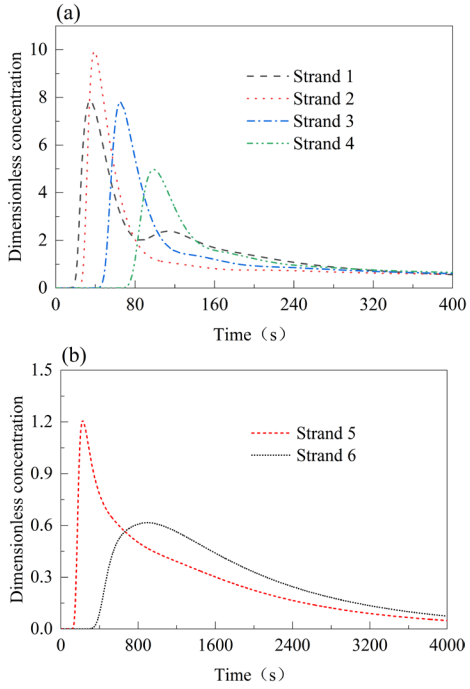

(a) Strand 1-4; (b) Strand 5-6

Fig. 6. RTD curves for each strand in case 1

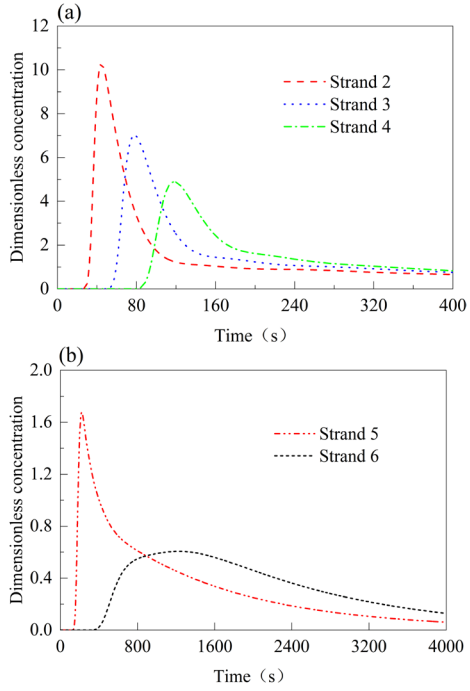

(a) Strand 1-4; (b) Strand 5-6

Fig. 7. RTD curves for each strand in case 2

For fewer strand operation in Case 2, as shown in Figure 7 and Table 3, the response time and peak concentration time at strands 2-4 gradually increase, which is slightly higher than that of Case 1. The peak concentrations varies slightly for the strands 2-4. Compared to Case 1, the peak concentration time at strand 5 decreases slightly, and the peak concentration increases to 1.68. This indicates an improvement in the flow at strand 5. The peak time at strand 6 increases significantly, rising from 888.8s in Case 1 to 1177.5s.

As shown in Figure 8 and Table 3, in Case 3, the flow characteristic parameters at strands 1, 3, and 4 are similar to that of Case 1. The peak concentration at strand 3 increases when compared with Case 1. Compared to Case 2, the minimum response time at strand 5 increases to 154.8s, and the peak concentration time significantly rises to 272.9s, while the peak concentration decreases to 1.28. Typically, for RTD curves with a sharp increase and decrease, the flow state at the outlet is short-circuit flow. While a slightly increasing RTD curve (positive sinusoidal) indicates the slow flow from the outlet. The observed extension in peak concentration time coupled with the reduction in peak concentration at strand 5 suggests a deceleration in the molten steel flow velocity. These flow characteristics demonstrate that the operational conditions implemented in Case 3 have adversely affected at strand 5. The peak concentration time at strand 6 is 958.5s, which decreases slightly compared to Case 2.

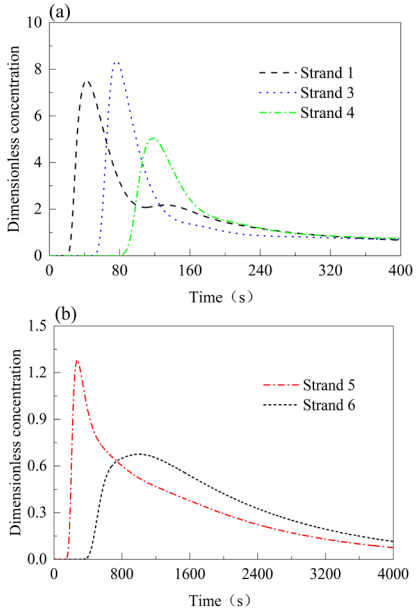

(a) Strand 1-4; (b) Strand 5-6

Fig. 8. RTD curves for each strand in case 3

As shown in Figure 9, in Case 4, the minimum response time and peak concentration time at strands 5 and 6 significantly increase when comparing the other cases. In conjunction with Figures 4(b) and 5, closing strand 1 and strand 2 in Case 4 leads to an increase in the slow-flow volume in the tundish, which worsens the flow of molten steel at far-side strand region.

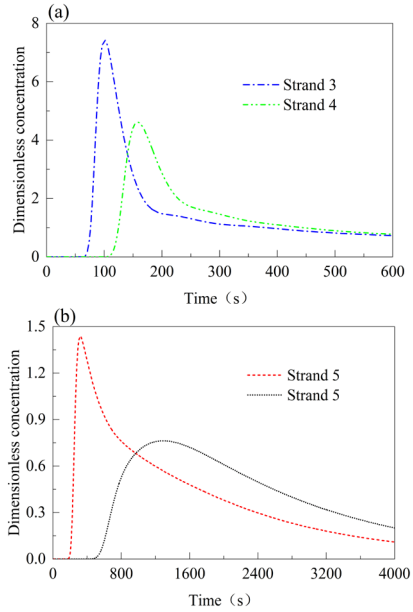

(a) Strand 1-4; (b) Strand 5-6

Fig. 9. RTD curves for each strand in case 4

In Case 1, the mean residence time exhibits a gradual increase from strand 1 to strand 6. Compared to Case 1, the mean residence time of each strand in Cases 2 and 3 increases, suggesting that the closure of individual strands leads to reduced flow velocity of molten steel. Notably, in Case 4, while strands 3 to 5 show decreased mean residence times compared to Case 3, strand 6 exhibits a substantial increase, reaching a maximum value of 1615.1 s.

3.3. Temperature Field in the Tundish

When new heat of ladle is poured into the tundish, its temperature is usually higher than that of the present heat. Figure 10 shows the temperature field in the tundish for each case during the pouring of new heat into present heat. A temperature difference exists between the higher-temperature new heat and the present heat. At 120s, the surface temperature in the impact area and near strand 1 is higher, while strands 2-4 form a temperature transition area. The free surface temperature ranges from 1701K to 1773K, and the temperature significantly drops at strands 5 and 6, where a lower temperature region exists. From the temperature distribution on the long wall, the temperature in Case 1 is around 1820K, while the temperature in Cases 2-4 show a gradually decreasing trend.

By monitoring the temperature of the molten steel flowing out from each strand, the temperature change curves as a function of time for each case are obtained, as shown in Figure 11. In practice, the weight of molten steel in ladle is 150 t, and the time for casting one heat is 28.3 minutes. The 1800 s is used for study and covers the casting time. As shown in Figure 11(a), in Case 1, when new heat is poured for 120 seconds, the temperatures at strands 1-4 gradually increases by 2-6 K. At strands 5 and 6, the steel remains as old molten steel in the previous heat with a temperature of 1793 K, which is 16 K lower than that at strand 1. With continuous casting of new heat, the temperature of each strand gradually rises. The temperatures of strands 2 and 3 tend to be consistent and they are overlapped in figure 11(a). While the temperature of strand 5 increases rapidly at 180s, and the temperature of strand 6 rises at 300s. At 532s, the maximum temperature difference between strands 1 and 6 is 30.9K.

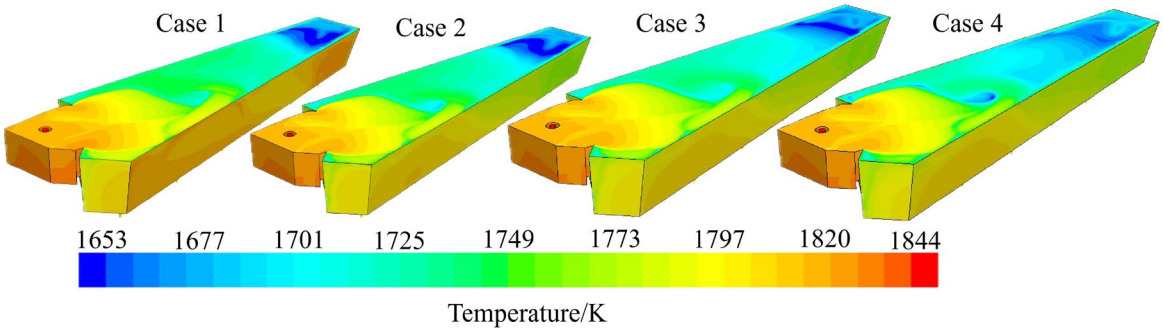

Fig. 10. Tundish temperature field after pouring 120s for each case

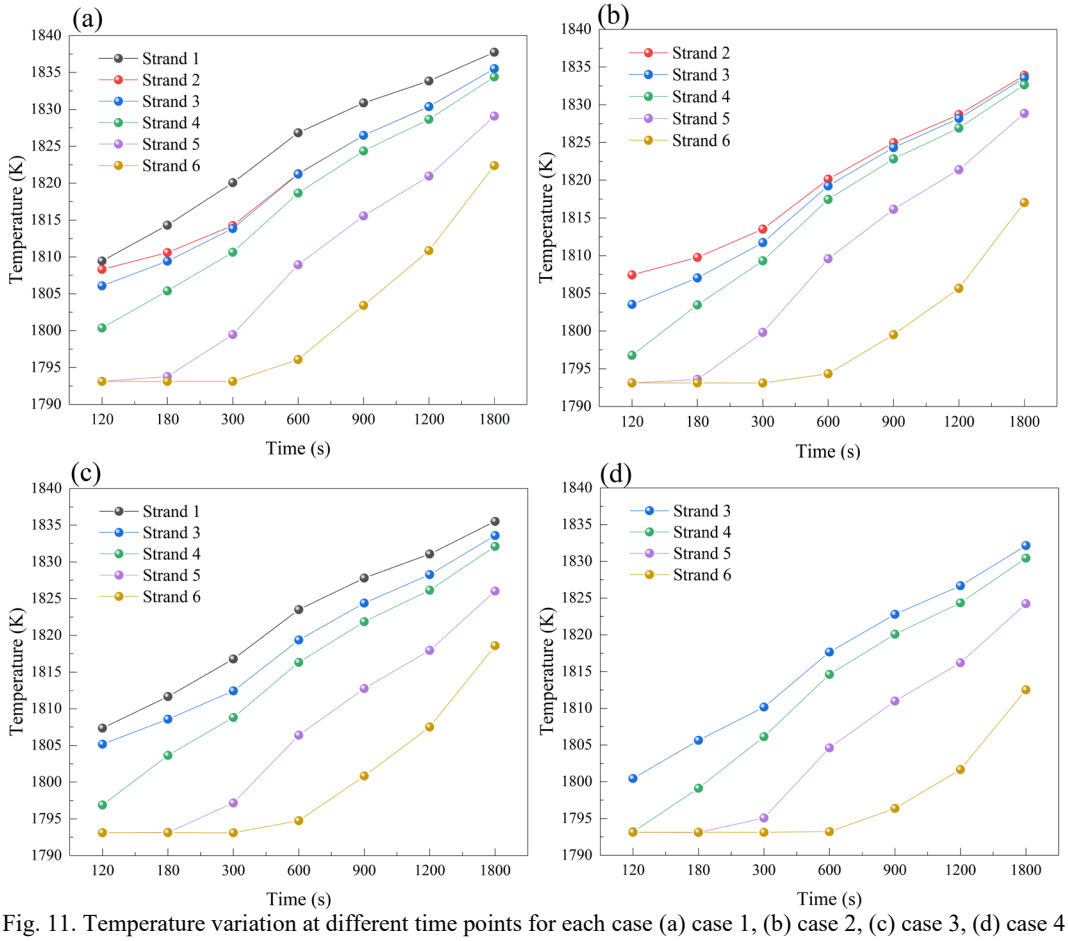

Fig. 11. Temperature variation at different time points for each case (a) case 1, (b) case 2, (c) case 3, (d) case 4

As shown in Figures 11(b) and 11(c), the temperature curves of strands 2, 3, and 4 in Case 2 are generally more consistent than those of strands 1, 3, and 4 in Case 3. This indicates that the temperature field in Case 2 is more uniform. During the period from 180s to 300s after casting of new heat, the temperature of strand 5 in Case 2 increases from 1793.6K to 1799.8K, while in Case 3, the temperature of strand 5 increases from 1793.2 K to 1797.2 K. The temperature increase in Case 3 is slightly smaller than that in Case 2. Additionally, in Case 2, the temperature difference between strands reaches a maximum value of 26.1 K at 702s, while in Case 3, the temperature difference reaches the maximum value of 28.7 K at 601s. The maximum temperature difference in Case 2 and Case 3 is smaller than in Case 1.

As shown in Figure 11(d), in Case 4, the maximum temperature difference between strands 3 and 6 is 26.4 K at 870s. At 1200s, the temperature of strand 6 in Case 4 is 1801.6K, which is 4 to 7 K lower than that in the other cases. At 1800s, the temperature is 1812.5K, which is 5 to 10 K lower than that in the other cases.

3.4. Impact of Fewer Strands Casting on Transition Billet Length

In this study, the concentration difference ratio of 20% to 80% between two heats as the standard for grade transition billet, as shown in Figure 12. A concentration difference ratio below 20% is considered as the composition of the old grade, while a concentration difference ratio above 80% is considered as the composition of the new grade. The range between 20% and 80% represents the transition billet.

The calculated transition billet length for each case are shown in Table 4. In Case 1, the transition billet length at strand 1 is 52.13m, and the lengths at strands 2, 3, and 4 are ranged from 66 to 72m. The transition billet lengths at strands 5 and 6 are close to 88m. The average transition billet length of all strands is 72.41m. Overall, the transition billet length at strands 5 and 6 is too long.

In Case 2, the transition billet lengths at strands 2, 3, and 4 are between 63 and 65m, while the lengths at strands 5 and 6 are 74.16m and 84.41m, respectively. The average transition billet length is 70.16m. Compared to Case 1, the transition billet length at strand 5 is reduced by 13.01m. The results indicate that fewer strands casting can reduce transition billet lengths to some extent.

Table 4.
Transition billet length of different strands for each case (m)

Case	Strand 1	Strand 2	Strand 3	Strand 4	Strand 5	Strand 6	Average length
Case 1	52.13	68.04	66.41	72.01	87.17	88.70	72.41
Case 2		63.48	62.23	65.5	74.16	84.71	70.16
Case 3	54.60		63.45	68.01	81.63	83.83	70.30
Case 4			55.55	59.38	70.29	76.59	65.45

This is because closing strand 1 prevents new heat of molten steel from quickly exiting through strand 1, at the same time the concentration of new heat of steel increases at the other strands.

In Case 3, the transition billet length at strand 1 is 54.60m, which is slightly increased when compared to that in Case 1. While the lengths at strands 3 and 4 are 63.45m and 68.1m, respectively. They are slightly decreased when compared to that in Case 1. The transition billet length at strand 5 is 81.63m, which is lower than that in Case 1, but it is 7.47m longer than that in Case 2. The average transition billet length in Case 3 is 70.30m, which is very close to than in Case 2.

In Case 4, since strands 1 and 2 are completely closed, the molten steel of new heat can exit at higher fractions through the far-side strands. As a result, the transition billet lengths at all strands in Case 4 are significantly reduced. The transition billet length at strands 4 and 5 are between 55 and 59m, and the length at strands 5 and 6 are ranged from 70 to 76m. The average transition billet length in Case 4 is 65.45m, which is reduced significantly than that in the other cases.

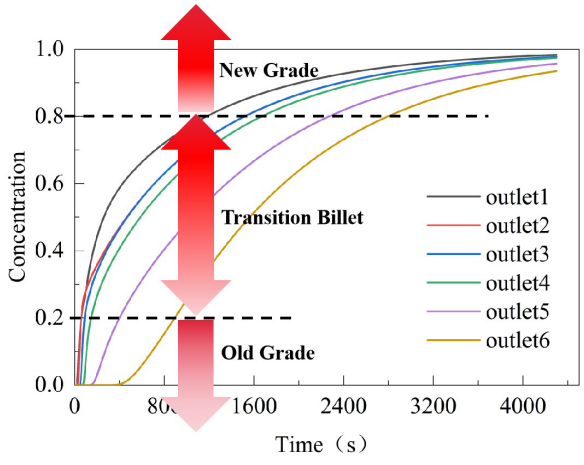

Fig. 12. Transition billet concentration-time curve at each strand during the grade transition casting process and schematic diagram for determining the new and old grade

4. Conclusions

1) Fewer strands casting in the 12-strand tundish slightly increases the slow-flow volume, which hinders molten steel flow at the far-side strands 5 and 6. The volume fraction of slow flow is Case1 < Case3 < Case2 < Case4. Based on the analysis of RTD curve and flow characteristic parameters, Case 2 performs better than Case 3 in fewer strands casting, while Case 4 significantly worsens the molten steel flow at the far-side strands.
2) The maximum temperature differences between different strands in each case are 30.9K, 26.1K, 28.7K, and 26.4K, respectively. In Case 2, the temperature curve of the near-side strands is more consistent than that in Case 3. With closing the strand 1 and 2, the Case 4 shows a smaller maximum temperature difference, but the temperature curves of each strand are less consistent.
3) The average length of transition billets is Case4 < Case2 < Case3 < Case1. Both Case 2 and Case 3 show a reduction in transition billet length compared to the normal casting Case 1. The transition billet length at strand 5 in Case 2 is reduced by 7.47m compared to Case 3. Fewer strands casting operation prevents new heat of molten steel from flowing out from the near-side strands, thereby promoting an increase in the intermix of molten steel at the far-side strands.
4) Evaluated from the flow characteristics, temperature distribution, and length of transition billets, the Case 2 *i.e.* close strand 1 is the optimum case when closing one strand

in fewer strands casting operation. The closing of two strands is not recommended in this study.

Acknowledgements

The "14th Five Year Plan" for Education Science in Shanxi Province in 2024 (GH-240165) is acknowledged for financial support of this research.

References

[1] Szekely, J., Ilegbusi, O.J. (1989). *The physical and mathematical modeling of tundish operations*. Heidelberg: Springer.
[2] Sahai, Y. (2007). *Tundish technology for clean steel production.* World Scientific.
[3] Geng, M., Wang, T. & Chen, C. (2024). Assessment of the volume effect and application of an improved tracer in physical model of a single-strand bare tundish. *Metallurgical and Materials Transactions B*. 55(5), 4121-4131. https://doi.org/10.1007/s11663-024-03308-7.
[4] Cwudziński, A., Bul'ko, B. & Demeter, P. (2024). Numerical and physical modeling of steel flow behavior in the two strand tundish during nonconventional pouring conditions. *Archives of Foundry Engineering*. 24(4), 116-125. https://doi.org/10.24425/afe.2024.151319.
[5] Chen, L., Chen, J.S., Li, Y.Q., Wang, S.B. & Chen, C. (2020). On the ladle shroud design and mis-alignment effects on the fluid flow in a metallurgical tundish- a CFD model study. In *E3S Web of Conferences*. 185, 04069, 1-4. http://doi.org/10.1051/e3sconf/202018504069.
[6] Cao, J., Li, Y., Lin, W., Che, J., Zhou, F., Tan, Y., Li, D., Dang, J. & Chen, C. (2023). assessment of inclusion removal ability in refining slags containing Ce_2O_3. *Crystals*. 13(2), 202, 1-30. https://doi.org/10.3390/cryst13020202.
[7] Wang, T., Chen, C., Tao, X., Wang, J., Geng, M., Song, J., Li, L., Fan, J. & Lin, W. (2024). Impact of slag layer on macroscopic flow inside tundish and velocity near slag-steel interface. *The Chinese Journal of Process Engineering*. 24(9), 1058-1069. http://doi.org/10.12034/j.issn.1009-606X.224058.
[8] Wang, T., Wang, J., Chen, C., Chen, L., Geng, M., Song, J., Fan, J. & Lin, W. (2024). Physical and numerical study on right side and front side gas blowing at walls in a single-strand tundish. *Steel Research International*. 95(9), 2400037, 1-22. https://doi.org/10.1002/srin.202400037.
[9] Chen, C., Ni, P., Jonsson, L.T.I., Tilliander, A., Cheng, G. & Jönsson, P. G. (2016). A model study of inclusions deposition, macroscopic transport, and dynamic removal at steel-slag interface for different tundish designs. *Metallurgical and Materials Transactions B*. 47(2), 1916-1932. https://doi.org/10.1007/s11663-016-0637-6.
[10] Chen, C., Cheng, G.G., Yang, H.K. & Hou, Z.B. (2011). Physical modeling of fluid flow characteristics in a delta shaped, four-strand continuous casting tundish with different flow control devices. *Advanced Materials Research*. 284, 1071-1079. https://doi.org/10.4028/www.scientific.net/AMR.284-286.1071.
[11] Zhao, S., Zhu, S., Ge, Y., Wang, J., Xu, D., Li, Z. & Chen, C. (2023). Simulation of fluid flow and inclusion removal in five-flow t-type tundishes with porous baffle walls. *Metals*. 13(2), 215, 1-15. https://doi.org/10.3390/met13020215.
[12] Zhao, S., Lu, Z., Zhang, Z., Ma, Z., Cao, Y. & Tang, H. (2024). Formation factors of confluence vortex in double nozzle ladle at end of teeming. *Iron and Steel*. 59(05), 71-79. https://doi.org/10.13228/j.boyuan.issn0449-749x.20230579. (in Chinese)
[13] Zhang, J., Li, J. & Yang, S. (2014). Optimization of fluid flow in a twelve-strand continuous casting tundish with two strands closed. *Metalurgia International*. 19(4), 10-13.
[14] Zhang, L. (2005). Fluid flow, heat transfer and inclusion motion in a four-strand billet continuous casting tundish. *Steel Research International*. 76(11), 784-796. https://doi.org/10.1002/srin.200506097.
[15] Mishra, S.K., Jha, P.K., Sharma, S.C. & Ajmani, S.K. (2012). Effect of blockage of outlet nozzle on fluid flow and heat transfer in continuously cast multistrand billet caster tundish. *Canadian Metallurgical Quarterly*. 51(2), 170-183. https://doi.org/10.1179/1879139511Y.0000000032.
[16] Sengupta, A., Mishra, P., Singh, V., Mishra, S., Jha, P.K., Ajmani, S.K. & Sharma, S.C. (2013). Physical modelling investigation of influence of strand blockage on RTD characteristics in a multistrand tundish. *Ironmaking Steelmaking*. 40(3), 159-166. https://doi.org/10.1179/1743281212Y.0000000054.
[17] Merder, T. (2014). Numerical investigation of the hydrodynamic conditions in a multi-strand CC tundish with closed outlets. *Archives of Metallurgy and Materials*. 59(3), 887-892. https://doi.org/10.2478/amm-2014-0150.
[18] Wang, X., Wang, S., Hu, H., Xie, X., Wu, C., Chen, D. & Long, M. (2023). Flow behavior of liquid steel in fewer strands casting of six-strand bloom tundish. *Metals*. 13(4), 706, 1-15. https://doi.org/10.3390/met13040706.
[19] Fan, J., Li, Y., Chen, C., Ouyang, X., Wang, T. & Lin, W. (2022). Effect of uniform and non-uniform increasing casting flow rate on dispersion and outflow percentage of tracers in four strand tundishes under strand blockage conditions. *Metals*. 12(6), 1016, 1-28. https://doi.org/10.3390/met12061016.
[20] Song, J., Luo, Y., Li, Y., Guo, Z., Wang, T., Geng, M., Lin, W., Fan, J. & Chen, C. (2024). Comparison of fluid flow and tracer dispersion in four-strand tundish under fewer strand casting and sudden blockage of strand conditions. *Metals.* 14(5), 571, 1-32. https://doi.org/10.3390/met14050571.
[21] Ramstorfer, F. & Delane de Souza, M. (2022). Reduction of incompatible intermixing of different steel grades in continuous casting by optimizing the casting sequence. *International Journal of Cast Metals Research*. 35(3), 43-50. https://doi.org/10.1080/13640461.2022.2078550.
[22] Tsai, M.C. & Green, M. J. (1991). A three-dimensional concurrent numerical simulation of molten steel behavior and chemical transition at inland steel's No. 2 caster tundish. *In Steelmaking Conference Proceedings*. 74, 501-504.
[23] Yeh, J.L., Hwang, W.S. & Chou, C.L. (1993). The development of a mathematical model to predict composition

distribution in casting slab and intermix slab length during ladle changeover period and its verification by physical model. *ISIJ International.* 33(5), 588-594. https://doi.org/10.2355/isijinternational.33.588.

[24] Chen, H.S. & Pehlke, R.D. (1996). Mathematical modeling of tundish operation and flow control to reduce transition slabs. *Metallurgical and Materials Transactions B.* 27(5), 745-756. https://doi.org/10.1007/BF02915603.

[25] Guarneros, J., Morales, R.D. & Gutierrez, E. (2023). Optimized fluid flow control system for a tundish used in frequent steel grade change operations. *Steel Research International.* 94(6), 2200809, 1-17. https://doi.org/10.1002/srin.202200809.

[26] Xu, D., Rogler, J.P., Heaslip, L.J., Dorricott, J. D., Foss, R. (2002). Dynamic flow behavior in the tundish: optimization of grade transitions. In 60th Electric Furnace Conference, 10-13 November 2002 (pp.745-754). San Antonio, Texas, USA.

[27] Amorim, L.L., Silva, C.A., Resende, A.D., Silva, I.A. & Oliveira, M.J. (2018). A study of intermix in a six-strand billet caster. *Metallurgical and Materials Transactions A*. 49, 6308-6324. https://doi.org/10.1007/s11661-018-4915-6.

[28] Cwudziński, A., Pieprzyca, J. & Merder, T. (2023). Numerical and physical modeling of liquid steel asymmetric behavior during non-isothermal conditions in a two-strand slab tundish-"Butterfly Effect". *Materials*. 16(21), 6920, 1-18. https://doi.org/10.3390/ma16216920.

[29] Burns, M.T., Schade, J., Brown, W.A. & Minor, K.R. (1992). Transition model for armco steel's ashland slab caster. *Iron steelmaker*. 19(11), 35-39. ISSN: 0275-8687.

[30] Song, S., Sun, Y. & An, H. (2023). Numerical modeling of grade mixing and inclusion entrapment in eight strand billet tundish. *Metallurgical Research & Technology*. 120(1), 112-127. https://doi.org/10.1051/metal/2023006.

[31] Song, S., Sun, Y. & Chen, C. (2024). Numerical simulation of macro-segregation phenomena in transition blooms with various carbon contents. *Metals.* 14(3), 263, 1-19. https://doi.org/10.3390/met14030263.

[32] Song, S., Sun, Y., Zhou, W., Yang, J. & Yang, W. (2024). The effect of steel grade casting sequence on the length of transition bloom. *Metallurgical and Materials Transactions B*. 55(3), 1795-1811. https://doi.org/10.1007/s11663-024-03067-5.

[33] Ren, M., Zhi, J., Fan, Z., Wang, R., Chen, Y. & Yang, J. (2023). Influence of ladle exchange on inclusions in transition slabs of continuous casting for automotive exposed panel steel. *Metals*. 13(2), 404, 1-18. https://doi.org/10.3390/met13020404.

[34] Hou, Z., Cheng, G., Wu, C. & Chen, C. (2012). Time-series analysis technologies applied to the study of carbon element distribution along casting direction in continuous-casting billet. *Metallurgical and materials transactions B.* 43(5). 1517-1529. https://doi.org/10.1007/s11663-012-9732-5.

[35] He, F., Wang, H. & Zhu, Z. (2019). Numerical investigation of effect of casting speed on flow characteristics of molten steel in multistrand tundish. *ISIJ International*. 59(7), 1250-1258. https://doi.org/10.2355/isijinternational.ISIJINT-2018-835.